

Transmission and focusing of light in one-dimensional periodically nanostructured metalsF. J. García-Vidal,¹ and L. Martín-Moreno²¹*Departamento de Física Teórica de la Materia Condensada, Facultad de Ciencias (C-V), Universidad Autónoma de Madrid, E-28049 Madrid, Spain*²*Departamento de Física de la Materia Condensada, ICMA-CSIC, Universidad de Zaragoza, E-50015 Zaragoza, Spain*
(Received 30 October 2001; published 17 October 2002)

In this paper we show how the optical properties of a metallic film can be tailored by one-dimensional periodically nanostructuring it which, in turn modifies the surface plasmon properties. The interaction of light with the surface plasmons can be used for two apparently opposite effects: trapping incident radiation into small volumes (in reflection gratings) and transmitting light very efficiently (in transmission gratings). A physical picture of the mechanisms involved, as well as dependences of the transmission and reflection spectra on wavelength, absorption and geometrical parameters of the grating, are provided.

DOI: 10.1103/PhysRevB.66.155412

PACS number(s): 78.66.Bz, 73.20.Mf, 42.79.Dj, 71.36.+c

I. INTRODUCTION

The dielectric response of a metal is mainly governed by its free electron plasma. Within the Drude formalism, the frequency (ω)-dependent dielectric constant of a metal can be written as

$$\epsilon(\omega) = 1 - \frac{\omega_p^2}{\omega(\omega + i\gamma)}, \quad (1)$$

where ω_p is the plasma frequency (typically around 10 eV), γ is the absorption, and ω stands for the frequency. For frequencies smaller than the plasma frequency the real part of $[\epsilon(\omega)]$ is negative and, therefore, a metal behaves as a photonic insulator. A negative ϵ has another important consequence: a metal-dielectric interface is decorated with surface electromagnetic (EM) modes called surface plasmon polaritons (SPP's).¹ The dispersion relation of these modes, for a flat interface, is given by:²

$$k_x(\omega) = \frac{\omega}{c} \sqrt{\frac{\epsilon(\omega)}{\epsilon(\omega) + \epsilon_d}}, \quad (2)$$

where k_x is the momentum in a direction (x) parallel to the interface, c is the speed of light in vacuum, and ϵ_d is the dielectric constant of the dielectric medium.

As it has been described in many papers,² there is no crossing between the SPP dispersion relation [Eq. (2)] and the light cone; therefore, SPP's on a flat metal surface cannot be excited by an incident plane wave. However, if the metal-dielectric interface is periodically modulated, the folding of SPP bands allows SPP's to be excited by external radiation.

The aim of this paper is to show how a metal structured with a one-dimensional (1D) periodic modulation can be used for two opposite purposes: trapping incident radiation into very small volumes in reflection gratings with very narrow grooves [see Fig. 1(a)] or transmitting light very efficiently in transmission gratings of very narrow slits [see Fig. 1(b)]. We will show how both phenomena are linked to the excitation of surface plasmons.

Already in 1902, Wood³ reported the appearance of remarkable absorption anomalies in the reflectance spectra of

smooth metallic gratings illuminated by p -polarized light (E field perpendicular to the grating). These anomalies were definitely associated by Fano to the excitation of SPP's.⁴ Many years ago, Hessel and Oliner⁵ published a key paper about the optical anomalies of metallic gratings. They found two different types of anomalies: one attributed to the usual propagating SPP's already mentioned, and another one, specific of deep gratings and associated to standing waves, with a photon energy highly concentrated inside the grooves. The relation of the EM resonances appearing in deep reflection gratings with nonlinear optical effects observed in certain rough surfaces has been studied during the last 20 years, mainly in connection with the surface enhanced Raman effect.⁶ Experimental evidence for the existence of these localized modes at optical frequencies has been reported recently.⁷

Additionally, the emergence of the concept of photonic crystals in the late 1980's has sprung new studies of metallic gratings, as examples of 1D periodic dielectric media.⁸ Also very recently, several theoretical studies have appeared on the excitation of waveguide resonances in zero-order metal sinusoidal gratings,⁹ similar to the ones observed in gratings with rectangular grooves.

On the other hand, transmission gratings have not received so much attention, although some theoretical works have appeared in the past.^{10,11} However, since extraordinary optical transmission through a 2D hole array perforated on a metallic film was first reported four years ago,¹² there has been a renewed interest in analyzing the transmission properties of arrays of slits, that is, the 1D version of the structure studied by Ebbesen's group. Schroter and Heitmann¹³ and Treacy¹⁴ tried to fit the experiments on 2D hole arrays by analyzing 1D slit arrays with the same set of parameters. However, the comparison between transmission properties of slit and hole arrays has a very limited value, as there is a fundamental difference between them: in a slit waveguide there is always a propagating mode inside the channel, while in a hole waveguide there is a cutoff frequency and all modes are evanescent for (roughly) hole diameters smaller than half a wavelength. Therefore, wave propagation through the structure is radically different for those two systems.

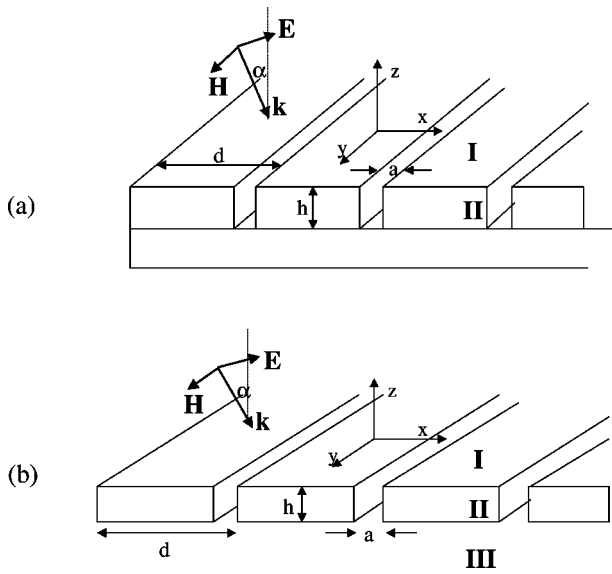


FIG. 1. Schematic view of the two types of nanostructured metals studied in this paper: (a) Reflection gratings with period d , grooves width a and depth h . (b) 1D arrays of narrow slits of width a separated by a distance d . Metal thickness in this configuration is h . In both cases we analyze the optical response of these systems to p -polarized light.

By analyzing the dependence of the transmission properties of arrays of slits with metal thickness, Porto *et al.*¹⁵ found that this kind of structures can be highly transmissive at certain wavelengths, larger than the period of the grating. Two types of transmission resonances were reported in this theoretical work: coupled SPP's on both horizontal surfaces of the metallic grating, and cavity modes located inside the slits. Recently, it was predicted¹⁶ that these cavity resonances are also present in a single narrow slit in a perfect metal. Subsequent theoretical studies of the complex band structure of transmission gratings¹⁷ have also revealed the presence of these two different types of resonances: coupled SPP's and cavity modes. Very recently, experiments in arrays of submillimeter slits have found enhanced transmission at certain microwave frequencies, through the resonant excitation of cavity modes.¹⁸

II. THEORETICAL FORMALISMS

In order to analyze the EM interaction of reflection and transmission gratings with external radiation we apply two different theoretical frameworks: (i) A transfer matrix formalism,¹⁹ with adaptable meshes,²⁰ which is necessary in order to be able to take into account the variation of EM fields at different lengthscales, typical of metallodielectric structures. This method yields virtually exact results, once convergence is obtained. (ii) A quasianalytical modal expansion, as described in Ref. 21, with two main simplifications: first, as we are interested in the optical response of a metal at frequencies well below its plasma frequency, surface impedance boundary conditions are imposed on the metallic surfaces. In this way, fields inside the metal need not be calcu-

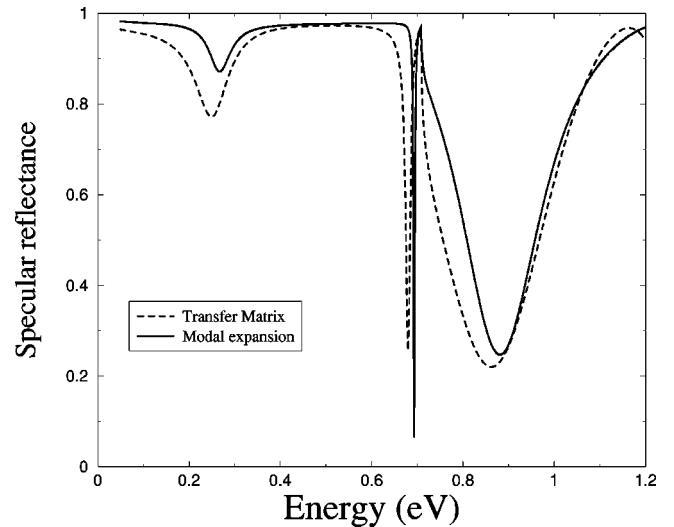


FIG. 2. Specular reflectance curves vs energy (in eV) of an incoming p -polarized plane wave impinging at normal incidence on a reflection grating with parameters: $d=1.75 \mu\text{m}$, $a=0.3 \mu\text{m}$, and $h=1.0 \mu\text{m}$. Dashed line corresponds to the theoretical curve obtained with the transfer matrix formalism whereas full line is the result of applying a quasianalytical modal expansion, as described in the text.

lated, its effect being reflected through a modification of the boundary conditions. Also, given that we are going to consider geometrical arrangements of grooves or slits where the "horizontal" metal-dielectric interface is much larger than the vertical one, we further simplify the model by assuming that the vertical walls of the grooves or slits are perfect metal surfaces. Relaxing this approximation would not change the physics, its main effect being just a small increase of the absorption by the metal. Second, as the wavelength of light is much larger than the lateral dimensions of the apertures, we only consider the fundamental eigenmode in the modal expansion of the EM fields inside the grooves or slits. This is justified because, in this regime, the fundamental mode is a propagating one and dominates the transmission as all other modes are evanescent. Considering more eigenmodes would, at most, slightly shift the frequency of the transmission features. The quasianalytical model is more convenient for understanding the transmission properties, specially after making the cited approximations, which render the model largely analytically tractable. In order to further justify the validity of these approximations and to evaluate the accuracy obtained by the modal expansion method, we show in Fig. 2 the comparison of specular reflectance curves for a reflection grating, for the case of p -polarized incident radiation impinging at normal incidence, obtained by both transfer matrix and modal expansion methods. The chosen parameters (in the range of what we are going to consider in this paper) are $d=1.75 \mu\text{m}$, $a=0.3 \mu\text{m}$, and $h=1.0 \mu\text{m}$ [see Fig. 1(a) for definitions]. The dielectric constant of the metal is assumed to be Drude-like [see Eq. (1)] with $\omega_p=9 \text{ eV}$ and $\gamma=0.1 \text{ eV}$. As clearly seen in the figure, specular reflectance spectra present dips for certain frequencies. These features are associated with the excitation of surface plasmons in the structure and will be analyzed in detail in Sec. III. The agree-

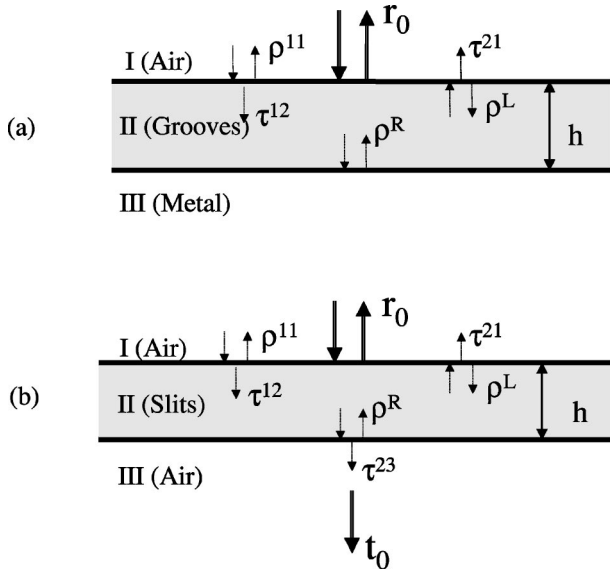


FIG. 3. Schematic definitions of the different scattering coefficients of the two independent two-region systems appearing in (a) reflection gratings and (b) transmission gratings (see the text).

ment between both methods is quite good; therefore, from now on, as we are mainly interested in understanding the fundamental optical properties of these systems, we only show results obtained with the quasianalytical modal expansion.

As previously stated, calculating the transmission or reflection amplitudes in the modal expansion method is a simple exercise of matching fields at different interfaces. Both reflection and transmission gratings are systems which can be decomposed in three different regions: the incident dielectric region (region I), the metal plus slits region (region II); and a third region, which is a semi-infinite metal in the case of reflection gratings and a semi-infinite dielectric in the case of transmission gratings. This means that the matching has to be done at two interfaces. However, for the systems we are considering, it is convenient to obtain the scattering coefficients in the three-region system from the scattering coefficients of two independent two-region systems: the I-II and the II-III systems, in which all regions are taken as semi-infinite (even region II). We define the scattering coefficients in the two-region systems as follow (see Fig. 3 to follow the definitions): In the I-II system, an incident plane wave coming from region I reflects, when reaching the I-II interface, with probability amplitude ρ^{11} or transmits through the interface with amplitude τ^{12} . The propagating mode inside the grooves (the only one considered in this case) approaching the II-I interface coming from region II, reflects with amplitude ρ^L , or transmits to region I with amplitude τ^{21} . Actually, ρ^{11} and τ^{21} would be vectors, given that the final state could be any of the diffraction orders. In this paper we are mainly interested in scattering properties for wavelengths larger than the lattice parameter, where only the zero diffraction order is propagating. Therefore, in order to calculate the total reflectance or transmittance, only the zero-order coefficients are needed and these are the ones the definitions are referring to. In the II-III system, the propagating mode com-

ing from region II bounces back at the II-III interface with amplitude ρ^R or transmits to region III with amplitude τ^{23} .

Given all these coefficients, the reflection and/or transmission coefficients for the real three-region system can be easily calculated summing up all multiple scattering processes, the only additional ingredient needed is the phase accumulated by the EM field when traveling inside region II. For the fundamental mode in 1D waveguides, this phase is \exp^{ik_0z} , where k_0 coincides with the wavevector modulus in vacuum and z is the distance traveled. The final result is

$$r_0 = \rho^{11} + \frac{\tau^{12} \exp^{2ik_0h} \rho^R \tau^{21}}{1 - \rho^L \rho^R \exp^{2ik_0h}} \quad (3)$$

for the specular reflection coefficient r_0 , and

$$t_0 = \frac{\tau^{12} \exp^{ik_0h} \tau^{23}}{1 - \rho^L \rho^R \exp^{2ik_0h}} \quad (4)$$

for the zero-order transmission coefficient. If a multimode expansion of the fields inside the slits were considered, very similar matricial expressions would be applicable.

All the “two-region” scattering magnitudes appearing in both Eqs. (3) and (4) can be calculated straightforwardly by just applying boundary conditions for electric and magnetic fields on the different interfaces. For the case in which the dielectric in regions I and III and the nonmetallic part of region II are all the same, with a dielectric constant equal to unity (the symmetric configuration), we find the expressions

$$\tau^{12} = \frac{2S_0 \cos \alpha}{\cos \alpha + Z_S} \frac{1}{1 + (1 - Z_S)f}, \quad (5)$$

$$\rho^{11} = \frac{\cos \alpha - Z_S}{\cos \alpha + Z_S} - \frac{2S_0 \tilde{S}_0 (1 - Z_S) \cos \alpha}{(\cos \alpha + Z_S)^2} \frac{1}{1 + (1 - Z_S)f}, \quad (6)$$

$$\rho^L = -\frac{1 - (1 + Z_S)f}{1 + (1 - Z_S)f}, \quad (7)$$

$$\tau^{21} = \frac{2\tilde{S}_0}{\cos \alpha + Z_S} \frac{1}{1 + (1 - Z_S)f}, \quad (8)$$

where α is the angle of incidence and $Z_S = \epsilon(\omega)^{-1/2}$ is the metal impedance. With respect to the other two-region scattering coefficients, which contain all the difference between transmission and reflection gratings, for the symmetric configuration we find, $\rho^R = \rho^L$ and $\tau^{23} = \tau^{21}$ for transmission gratings, whereas in the case of reflection gratings $\rho^R = [(1 - Z_S)/(1 + Z_S)] \approx 1$ and $\tau^{23} = 0$.

Functions S_n and \tilde{S}_n , with integer n , are essentially overlap functions between the incoming plane wave and the fundamental eigenmode inside region II,

$$S_n = \frac{\sin k_0 \gamma_n a/2}{k_0 \gamma_n a/2}, \quad (9)$$

with $\tilde{S}_n = (a/d)S_n$ and $\gamma_n = \sin \alpha + (2\pi n/k_0 d)$.

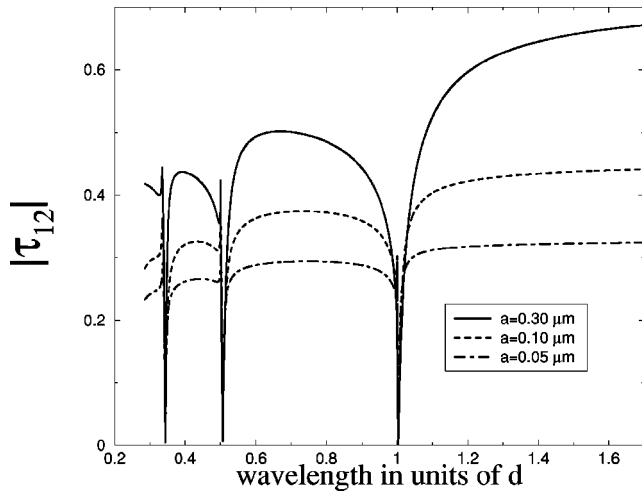


FIG. 4. Modulus of τ_{12} (probability amplitude for a normal incident p -polarized plane wave for being transmitted when reaching the I-II interface). τ_{12} is shown for three different values of the slits width (a) as a function of the wavelength (in units of d , which is $d = 1.75 \mu\text{m}$ in this case) for a normal incident plane wave.

Function f plays a key role in all scattering magnitudes, and can be written up as

$$f = \sum_{n=-\infty}^{\infty} \frac{S_n \tilde{S}_n}{(1 - \gamma_n^2)^{1/2} + Z_S}. \quad (10)$$

A crucial point, which will strongly influence reflection and transmission properties, is that f is singular when $(1 - \gamma_n^2)^{1/2} \rightarrow -Z_S$, which is just the condition of SPP existence on a flat metal surface.

Before analyzing the properties of reflection and transmission gratings, we show the dependence with wavelength of the “two-region” scattering coefficients. Figure 4 shows the dependence of $|\tau^{12}|$ with wavelength of incoming p -polarized light, for normal incidence. The grating period is $d = 1.75 \mu\text{m}$, and several values of a , ranging from 0.05 to 0.30 μm , are represented. As in Fig. 2, $\omega_p = 9 \text{ eV}$ and $\gamma = 0.1 \text{ eV}$. As seen in this figure, the transmission amplitude through the I-II interface is practically zero at SPP locations for normal incidence ($\lambda_{SPP} \approx d, d/2, d/3, \dots$). The other transmission magnitudes τ^{23} and τ^{21} appearing in Eq. (8) are also antiresonant at the SPP condition.

As a difference with the transmission magnitudes, ρ^L is resonant at the SPP condition: in Eq. (7) for $f \rightarrow \infty$, $\rho^L \approx 1$. Figure 5 shows the modulus of ρ^L (R) in panel (a), and its phase (θ) in panel (b), as a function of wavelength for the same set of parameters of Fig. 4. Both R and θ are singular at the SPP conditions: in the case of θ there is a phase jump from π to 2π when approaching SPP locations; these jumps are more abrupt when the width of the slits tends to zero. Other interesting point is that R approaches unity at the same SPP location. This result can be understood as follows: from Eq. (10), function f can be interpreted as the total “conductance” (inverse of impedance) of region I which is the sum of the conductances associated with all possible channels acting in parallel. When the conductance of one of these evanescent channels is infinite (at the SPP condition), this channel shortcuts transmission into region I, producing perfect reflection due to current conservation.

III. REFLECTION GRATINGS

First we analyze the case of reflection gratings with very narrow grooves. If we rewrite $\rho^L = R e^{i\theta}$, and neglecting the unimportant scattering phase at interface II-III, which is virtually 2π , the specular reflection amplitude r_0 [see Eq. (3)] can be expressed as

$$r_0 \approx \rho^{11} + \frac{\tau^{12} \exp^{2ik_0h} \tau^{21}}{1 - R \exp^{i\phi_R}}, \quad (11)$$

where ϕ_R is the sum of $2k_0h$ plus θ , which is the change in the phase of a propagating mode after reflecting on the II-I

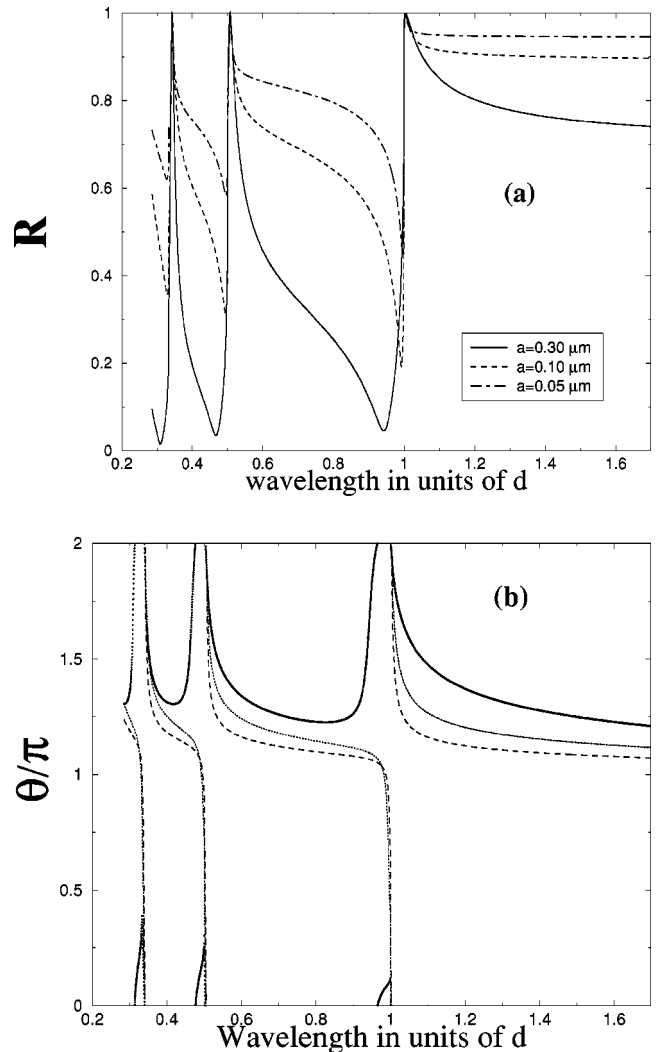


FIG. 5. Behavior of R (modulus of ρ^L , in the upper panel) and θ (phase of ρ^L , in the lower panel) vs the wavelength (in units of d) of a propagating mode inside region II impinging the II-I interface. Both magnitudes are displayed for different values of a and, as in previous cases, $d = 1.75 \mu\text{m}$.

When the conductance of one of these evanescent channels is infinite (at the SPP condition), this channel shortcuts transmission into region I, producing perfect reflection due to current conservation.

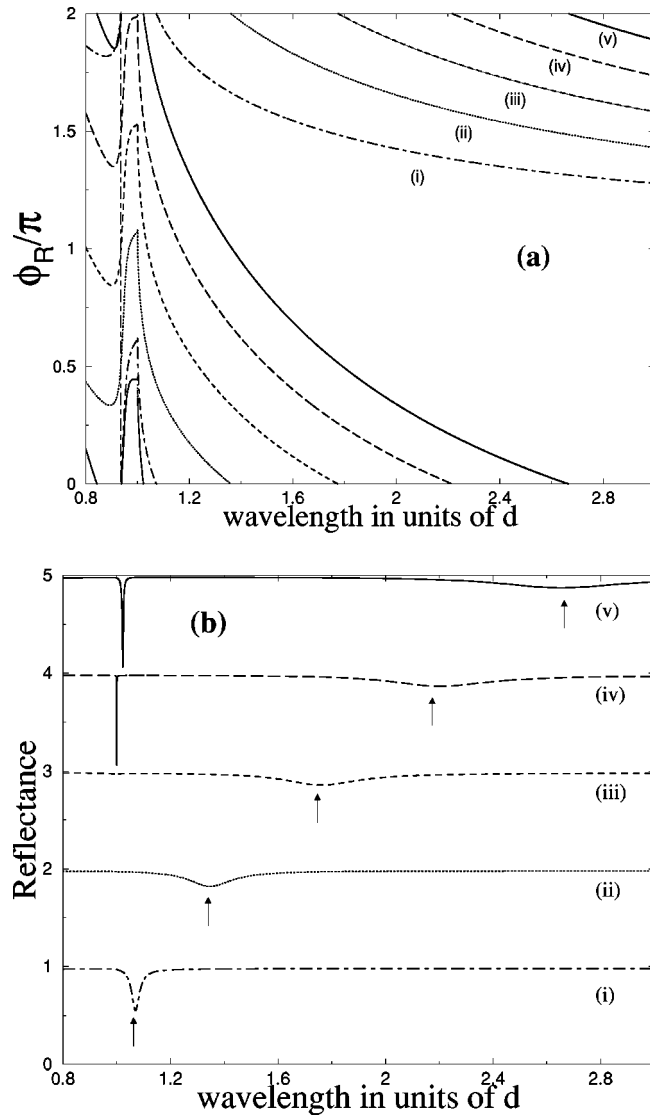


FIG. 6. Total phase ϕ_R [panel (a)] and specular reflectance spectra [panel (b)] as a function of wavelength for a normal incident plane wave impinging reflection gratings with $d=1.75 \mu\text{m}$ and $a=0.3 \mu\text{m}$ for different grooves depths: (i) $h=0.2 \mu\text{m}$, (ii) $h=0.4 \mu\text{m}$, (iii) $h=0.6 \mu\text{m}$, (iv) $h=0.8 \mu\text{m}$, and (v) $h=1.0 \mu\text{m}$. In panel (b) each curve is shifted by +1 with respect to the previous one for a better visualization.

interface. In order to distinguish it from $2k_0h$ that is the phase accumulated when traveling inside the waveguide, let us call θ the “scattering phase.” An interesting result is that the absorption properties of reflection gratings are completely governed by the total phase ϕ_R : whenever ϕ_R is an integer times 2π , there is a constructive interference between all partial reflected waves that tend to cancel ρ^{11} , provoking a dip in r_0 , indication that some energy is absorbed by the system, as there is no channel for transmission in this geometry.

In order to illustrate this result, Fig. 6 shows the relation between ϕ_R and the specular reflectance ($|r_0|^2$) as a function of wavelength, for reflection gratings with $d=1.75 \mu\text{m}$, $a=0.3 \mu\text{m}$, and several values of grooves depth (h , ranging

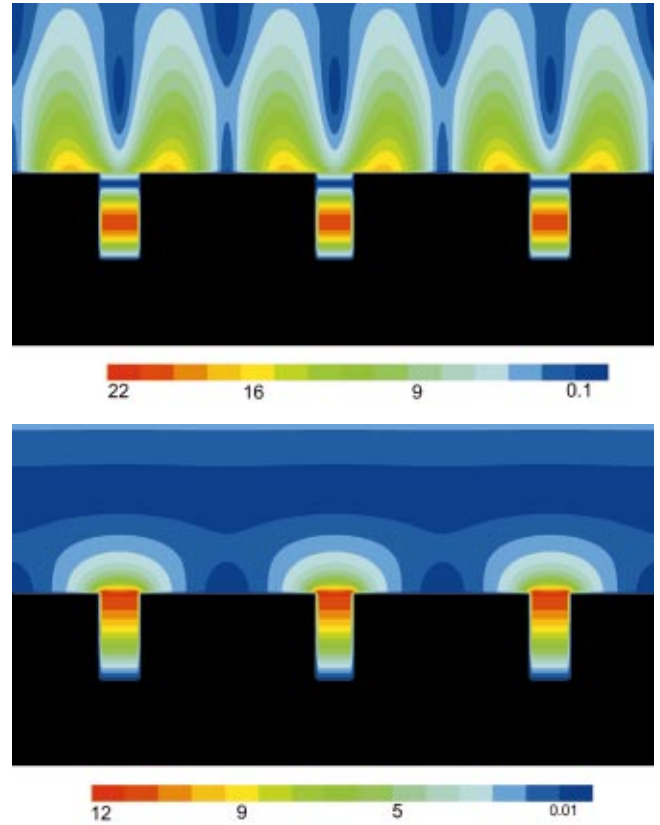


FIG. 7. (Color) Detailed pictures of the E field over three periods of reflection gratings with geometrical parameters $d=1.75 \mu\text{m}$, $a=0.3 \mu\text{m}$, and $h=1.0 \mu\text{m}$. The magnitude displayed in color scale is the square root of the intensity of the total E field normalized to the incoming E field. The two figures correspond to the two resonances appearing in the corresponding reflectance spectrum (see Fig. 6): (a) $\lambda_R=1.8 \mu\text{m}$ and (b) $\lambda_R=4.6 \mu\text{m}$.

from $h=0.2$ to $1.0 \mu\text{m}$). For small values of h [see, for example, $h=0.2 \mu\text{m}$, curve (i)], total phase is essentially equal to the scattering phase (θ). Therefore, the condition $\phi_R=2n\pi$ occurs very close to the SPP condition. Accordingly, specular reflectance spectrum shows a dip at a wavelength close to the SPP location. When h is increased, the condition $\phi_R=2n\pi$ occurs at longer wavelengths and, accordingly, the dip in the reflectance redshifts (see curves for $h=0.4$ and $0.6 \mu\text{m}$ in Fig. 6).

If we consider even deeper grooves, there is a critical thickness [for this particular set of parameters for $h \approx 0.8 \mu\text{m}$; see curve (iv) in Fig. 6] from which there are two wavelengths fulfilling $\phi=2n\pi$ and the reflectance shows two EM resonances: one located at a wavelength close to the SPP condition, and another one at a much longer wavelength. The locations of these cavity resonances at $\lambda \gg d$ can be easily calculated by realizing that, for this range of frequencies, $\theta \rightarrow \pi$, and then the condition $\phi_R=2n\pi$ is equivalent to $\sin k_0h=1$. If h is further increased, more cavity resonances will fit inside region II, as recently reported in very deep sinusoidal gratings.⁹

There is another interesting feature of these EM reso-

nances: associated with the absorption of light, and as a result of the excitation of these modes by external light, high focusing of light or E field enhancement in very small volumes appears, which could have applications in nonlinear optics or in surface enhanced Raman scattering. This focusing is illustrated in Fig. 7, which shows E -field pictures corresponding to the two EM resonances obtained for the case $d=1.75 \mu\text{m}$, $a=0.3 \mu\text{m}$ and $h=1.0 \mu\text{m}$: one resonance is located at $\lambda=1.8 \mu\text{m}$ (very near to the SPP condition) and the other one at $\lambda=4.6 \mu\text{m}$. The magnitude displayed in this figure is the square root of the ratio between the intensity of total E field and the intensity of the incoming field. As clearly seen in the figure, the resonance of longer wavelength is a cavity mode in which the E field is highly concentrated inside the grooves (with an E -field intensity enhancement of around 100) whereas in the upper case (shorter wavelength resonance), the intensity is an hybrid between that of a cavity mode and of a SPP, for which the energy is located on the outmost surface. In this last case, the intensity enhancement is even larger, of around 400. In general, the E -field intensity enhancement at resonance is basically controlled by the ratio d/a . It can be shown that for $\lambda > d$, the amplitude of the E field inside the grooves (A_0) is simply

$$A_0 \approx \frac{d}{a} \frac{e^{ik_0h}}{\sin k_0h} E_{inc}, \quad (12)$$

where E_{inc} is the amplitude of the incoming plane wave.

For cavity resonances ($\lambda \gg d$), $\sin k_0h=1$, giving an enhancement of the E -field intensity inside the grooves that is proportional to $(d/a)^2$. This enhancement is even larger for resonances located near the SPP condition, as in this case $\sin k_0h < 1$. Moreover, if the period of the grating (d) is tuned to twice the depth of the grooves (h), then $\sin k_0h \rightarrow 0$ and according to Eq. (12), extremely high electric fields associated to the excitation of these surface plasmons could be obtained. In this particular case, the E -field enhancement would only be limited by absorption.

The photonic band structure (energy versus momentum) of these surface plasmon resonances can be calculated by varying the angle of incidence (α) and analyzing when the condition $\phi_R = 2n\pi$ occurs. In Fig. 8 we show the resulting band structure for $d=1.75 \mu\text{m}$, $a=0.3 \mu\text{m}$, and for different values of h : (a) $h=0.05 \mu\text{m}$, (b) $h=0.2 \mu\text{m}$, (c) $h=0.6 \mu\text{m}$, and (d) $h=1.0 \mu\text{m}$. For small values of h [see Fig. 8(a)], the effect of the grooves on the SPP bands is just the appearance of minigaps located at $k_x=0$ and $k_x=\pi/d$.

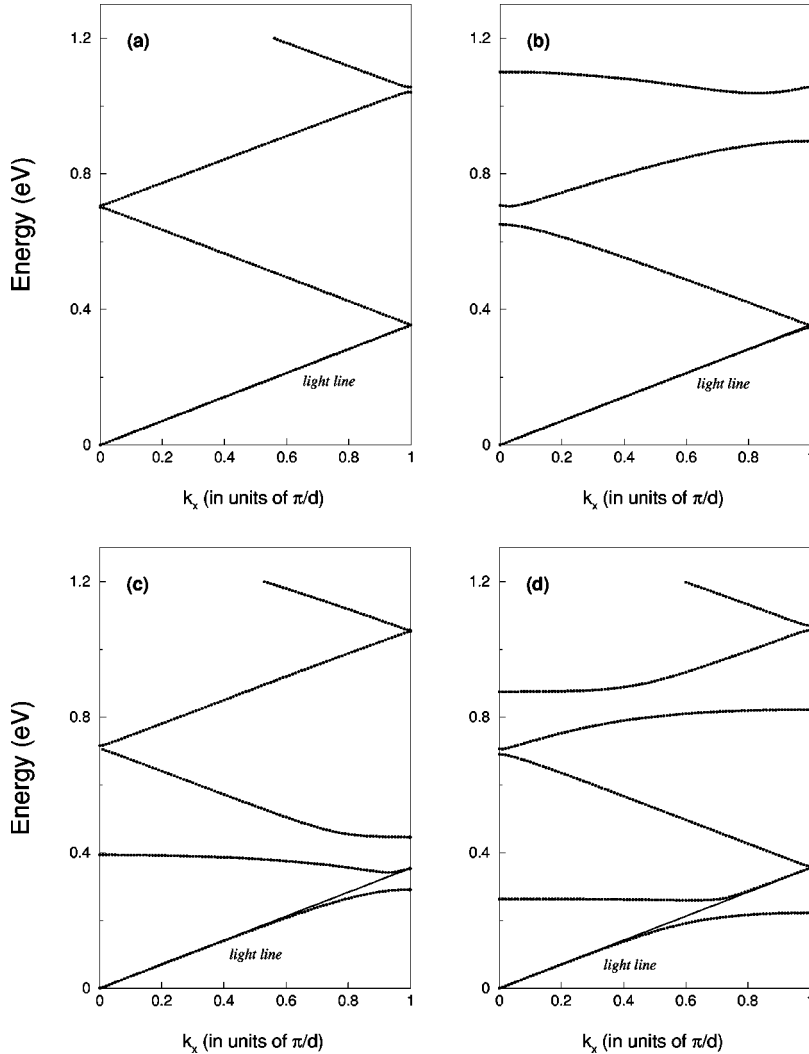


FIG. 8. Photonic band structure (black dots) of the surface plasmons associated to the EM resonances appearing in reflection gratings of period $d=1.75 \mu\text{m}$, $a=0.3 \mu\text{m}$ and different groove depths: (a) $h=0.05 \mu\text{m}$, (b) $h=0.2 \mu\text{m}$, (c) $h=0.6 \mu\text{m}$, and (d) $h=1.0 \mu\text{m}$.

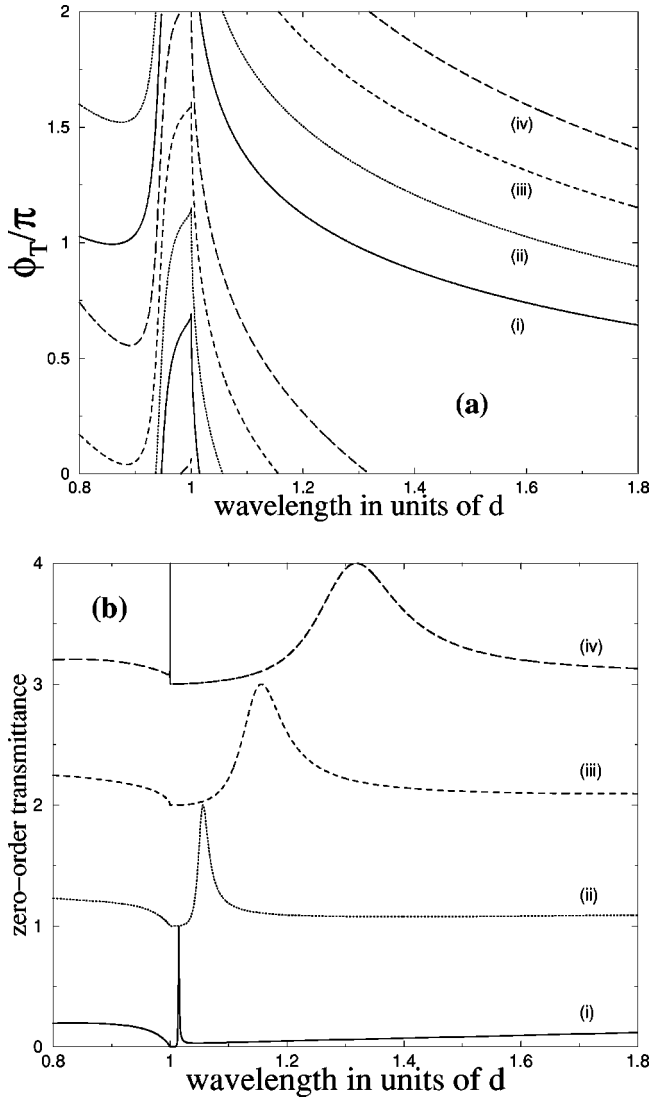


FIG. 9. Total phase ϕ_T in panel (a) and zero-order transmittance spectra in panel (b) as a function of wavelength for a normal incident p -polarized plane wave impinging on transmission gratings with $d=1.75 \mu\text{m}$ and $a=0.3 \mu\text{m}$, for different thicknesses: (i) $h=0.2 \mu\text{m}$, (ii) $h=0.4 \mu\text{m}$, (iii) $h=0.6 \mu\text{m}$, and (iv) $h=0.8 \mu\text{m}$.

For deeper grooves ($h=0.2 \mu\text{m}$), the perturbation is greater: the gap between the second and third bands has increased notably (note that the lower branch near the gap at $k_x=0$ corresponds to the dip in the reflectance curve observed in Fig. 6) and the fourth SPP band has changed radically from the almost flat surface (shallow grooves) case. This major change is due to the fact that this band is quite close in energy to the lowest energy cavity mode of a single groove of $h=0.2 \mu\text{m}$ that is located at 1.55 eV . Further increase in h provokes the energy lowering of these cavity resonances and, associated with this, the appearance of flat bands showing very little dispersion with parallel momentum. This implies that absorption of energy by these EM resonances is almost independent on the angle of incidence, feature which could be useful in some optical devices. For $h=0.6 \mu\text{m}$ [see Fig. 8(c)], the corresponding cavity mode is located at $E=0.52 \text{ eV}$ and this mode is the origin of the flat band present

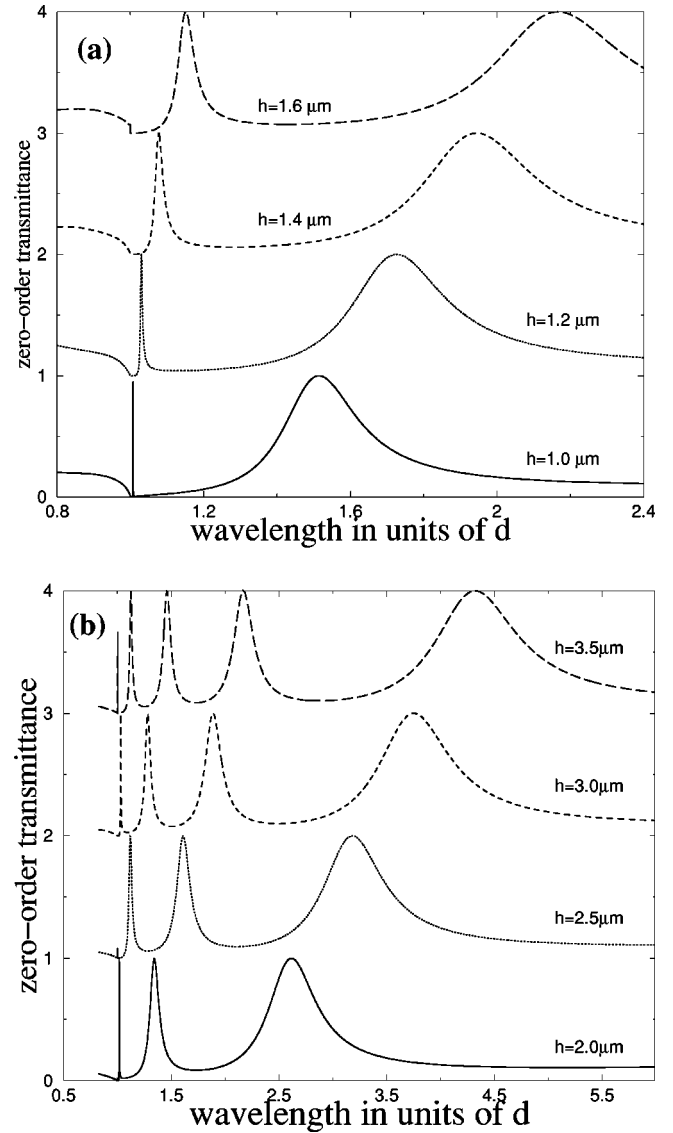


FIG. 10. Zero-order transmittance spectra as a function of wavelength for a normal incident p -polarized plane wave impinging on transmission gratings with $d=1.75 \mu\text{m}$ and $a=0.3 \mu\text{m}$, and different thicknesses, ranging from $h=1.0$ to $1.6 \mu\text{m}$ in panel (a) and from $h=2.0$ to $3.5 \mu\text{m}$ in panel (b).

at around 0.4 eV . Note that for this case, the third and fourth bands are almost identical to the SPP bands because, as opposed to the case shown in Fig. 8(b), they do not mix with the very low energy cavity mode. For very deep reflection gratings [$h=1.0 \mu\text{m}$; see Fig. 8(d)], the photonic band structure of the surface plasmons is just a combination of flat bands, associated with cavity resonances, and bands with basically SPP character.

IV. TRANSMISSION GRATINGS

Now we discuss transmission properties of an array of slits [see Fig. 1(b)]. As previously stated, we are mainly interested in the case $\lambda > d$, for which only the zero-order transmission coefficient t_0 [see Eq. (4)] contributes to the

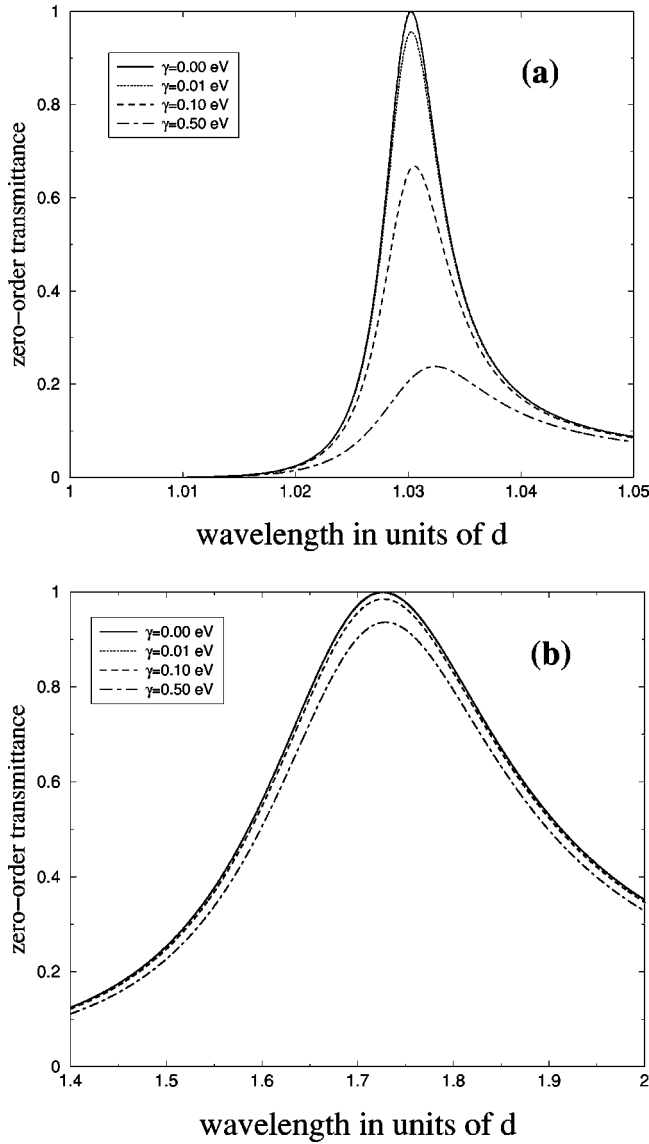


FIG. 11. Zero-order transmittance spectra as a function of wavelength for a normal incident p -polarized plane wave impinging on transmission gratings with $d=1.75 \mu\text{m}$, $a=0.3 \mu\text{m}$, and $h=1.2 \mu\text{m}$ for different values of γ , ranging from $\gamma=0$ to $\gamma=0.5 \text{ eV}$. Each panel shows the behavior as a function of damping in the metal of the two corresponding transmission resonances appearing for this set of geometrical parameters [see Fig. 10(a)].

transmitted current. For a symmetric situation ($\rho^R = \rho^L = R e^{i\theta}$) t_0 can be written as

$$t_0 = \frac{\tau^{12} \exp^{ik_0 h} \tau^{23}}{1 - R^2 \exp^{i\phi_T}}, \quad (13)$$

where $\tau^{23} = \tau^{21}$, given by Eq. (8), and the total phase $\phi_T = 2k_0 h + 2\theta$. As in the case of absorption in reflection gratings, transmission properties of a 1D array of slits are completely governed by ϕ_T . Given that for narrow slits $R \approx 1$, whenever ϕ_T is an integer times 2π the denominator of Eq. (13) is resonant and, accordingly, there is a peak in the transmittance spectrum. This close relation between total phase

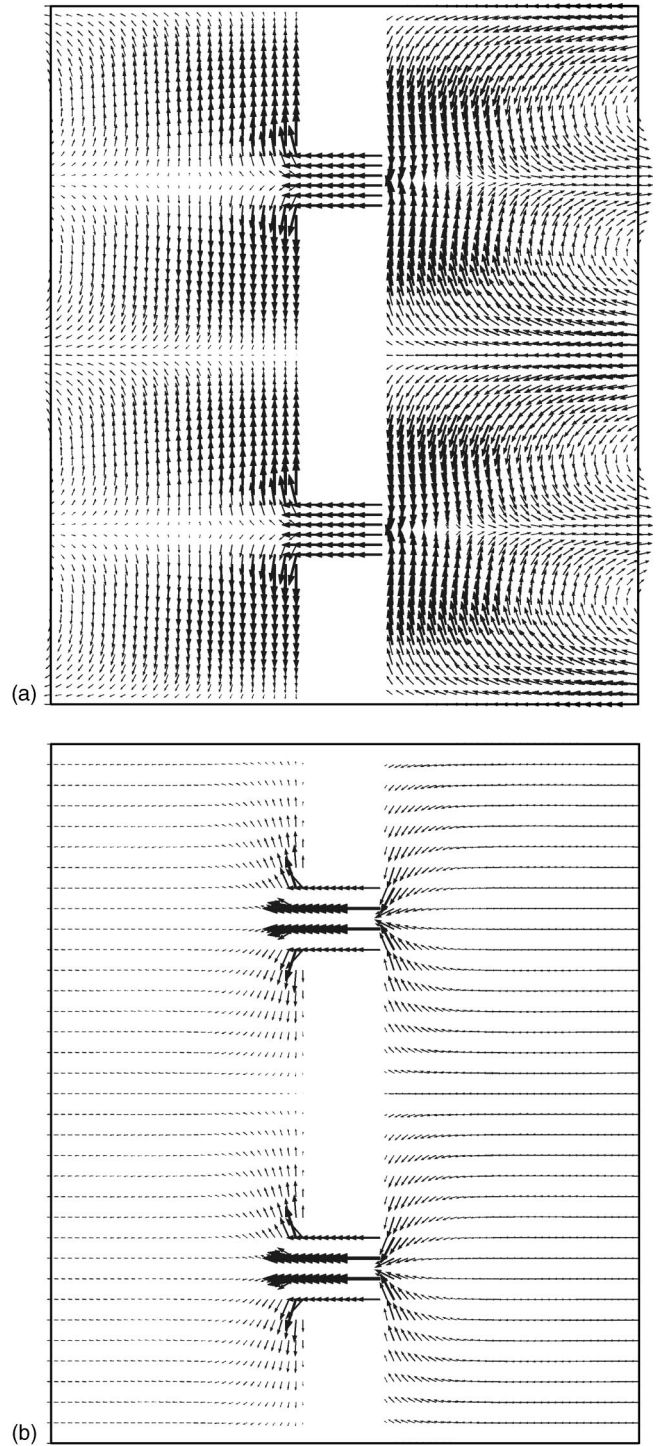


FIG. 12. Poynting vector ($\mathbf{S} = \mathbf{E} \times \mathbf{H}$) for a slit array with $d = 1.75 \mu\text{m}$ and $a = 0.3 \mu\text{m}$, for two different cases: (a) $h = 0.4 \mu\text{m}$ for $\lambda = 1.84 \mu\text{m}$, which is the resonant wavelength for this case [see Fig. 9(b)], and (b) $h = 1.2 \mu\text{m}$ for the resonant wavelength $\lambda = 3.0 \mu\text{m}$, that is linked to the excitation of a cavity mode [see Fig. 10(a)]. In this picture, light is impinging the 1D array of slits from the right.

and transmission (as in a Fabry-Perot interferometer) is illustrated in Fig. 9, which displays ϕ_T (upper panel) and $|t_0|^2$ (lower panel) as a function of wavelength of the incoming normal incident p -polarized plane wave, for the cases d

$=1.75 \mu\text{m}$ and $a=0.3 \mu\text{m}$ and for different values of the metal thickness h . In contrast to reflection gratings, where considering absorption is essential (otherwise $r_0=1$ for all $\lambda>d$, due to current conservation), transmission spectra in transmission gratings present structure even for lossless metals. In order to analyze this structure, we start by neglecting damping processes in the metal, i.e., $\gamma=0$. For thin metal films (see the panel for $h=0.2 \mu\text{m}$), $\phi_T \approx 2\theta$, and then the spectral location of the transmission resonance (in which the transmittance is 100%) is near the SPP location (remember that the scattering phase changes by π close to the SPP wavelength). When h is increased, the condition $\phi_T=2n\pi$ is fulfilled at longer wavelengths and, correspondingly, the resonance redshifts (see cases $h=0.4\text{--}0.6 \mu\text{m}$ in Fig. 9). This resonance also exhibits a perfect transmittance. Considering thicker metal films, there is a critical width ($h=0.8 \mu\text{m}$, for this set of parameters), for which the condition $\phi_T=2n\pi$ is satisfied at two different wavelengths. Correspondingly the transmittance spectrum shows two peaks, a very narrow one located near the SPP condition and another (much broader) one at around $1.3d$. These two resonances, appearing in the $h=0.8 \mu\text{m}$ case, illustrate the two different mechanisms that can lead to almost perfect transmittance of light in 1D arrays of slits, first reported in Ref. 15: excitation of coupled SPP's on both surfaces of the metallic gratings ($\lambda \approx d$) and cavity resonances ($\lambda > d$). Other authors (see Collin *et al.*¹⁷) preferred to identify them as horizontal and vertical surface-plasmon resonances, respectively. In any case, there is not always a clear distinction between these two ways of transferring light from the upper surface to the lower one: when h is further increased [see Fig. 10(a), $h=1.0\text{--}1.6 \mu\text{m}$), the resonance located near the SPP location for $h=0.8 \mu\text{m}$ moves to longer wavelengths, its character changing continuously, and becoming more like a cavity resonance for deeper gratings. In the limit of very deep transmission gratings ($h \gg d$), many different transmission resonances appear [see Fig. 10(b)], associated with the excitation of several cavity modes inside the slits. This behavior has been recently observed experimentally in transmission gratings built in the millimeter regime.¹⁸

At this point it is interesting to compare transmission properties of 1D array of slits with the extraordinary optical transmission observed in 2D hole arrays.¹² As commented upon earlier, the main difference between hole and slit arrays is that in this last case there is always a propagating mode inside the channel. Therefore, light inside the slits can travel back and forth between the two interfaces and the constructive interference between all partial transmitted waves can lead to transmission resonances, in a way very much similar to a conventional Fabry-Perot interferometer. However, in 2D hole arrays this process cannot occur because all waves inside the holes are evanescent. As discussed in Ref. 22, the enhancement of transmission in hole arrays is due to tunneling through the surface plasmons formed on each metal-dielectric interface. For thin films, both surface plasmons interact leading to resonant transmission through "surface plasmon molecule" levels, whereas for thick enough films optical tunneling is sequential through two isolated surface plasmons.

Going back to 1D slit arrays, it is worth analyzing the linewidths of the two types of resonances (coupled SPP's and cavity modes): it can be demonstrated that the linewidths of these resonances are inversely proportional to the derivative of ϕ_T with respect to λ . As seen in Fig. 9(a), the scattering phase does not change much with wavelength, except close to the SPP location, where it presents a very abrupt derivative [a footprint of the behavior of the scattering phase versus wavelength; see Fig. 5(b)]. This explains why the linewidth of the resonance widens as its wavelength location moves away from the SPP location. Linewidths also provide information about the sensitivity of these resonances to the presence of damping processes in the metal: coupled SPP's resonances will be extremely sensitive to γ [its associated transmittance is strongly reduced as γ is increased, as shown in Fig. 11(a)], whereas cavity resonances are very insensitive to γ [see Fig. 11(b)], and then can lead to almost perfect transmittance for realistic values of γ .

In order to visualize the transmission process associated with the excitation of different EM resonances of arrays of slits, Fig. 12 shows the Poynting vector ($\mathbf{S}=\mathbf{E} \times \mathbf{H}$) for an array of slits with $d=1.75 \mu\text{m}$ and $a=0.3 \mu\text{m}$, for two different cases: (a) $h=0.4 \mu\text{m}$ for $\lambda=1.84 \mu\text{m}$ which is the resonant wavelength for this case [see Fig. 9(b)], and (b) $h=1.2 \mu\text{m}$ for the resonant wavelength $\lambda=3.0 \mu\text{m}$ (see Fig. 10). Panel (a) shows how the transmission process is accompanied by the excitation of SPP's on both horizontal surfaces and, accordingly, the flow of energy is mainly along the metal-vacuum interfaces. In the situation depicted in panel (b), the system acts as like a funnel collecting all the energy impinging the structure and then "squeezing" it through the slits. In both cases, the transmission process is accompanied by a high focusing of the E field: in case (a) focusing occurs on both interfaces, whereas in case (b) the focusing occurs inside the slits.

In conclusion we have shown how, by periodically nanostructuring a metal surface, the resulting surface plasmons can be tailored in order to modify the optical properties of a metallic slab. By cutting very narrow and deep grooves in a metallic film it is possible to focus light into very small volumes for certain frequencies. As a result of this focusing, the E field is strongly enhanced, this enhancing capability depending basically on the ratio between the groove width and the grating period. The frequencies of the surface plasmon resonances that are responsible for this effect can also be tuned by choosing the appropriate set of geometrical parameters. On the contrary, if we want to use a metallic slab as a filter, the idea is to create a 1D array of narrow slits on the film. For certain wavelengths the system will be highly transmissive and, as in the previous case, this ability is linked to the excitation of surface plasmons, which are able to collect most of the incoming energy and to reemit it in the forward direction. Also these transmission capabilities can be controlled by geometry (period, slits width, and metal thickness).

ACKNOWLEDGMENT

We acknowledge financial support from the Spanish CICYT under Contract No. BFM2000-1319-C02.

- ¹R.H. Ritchie, Phys. Rev. **106**, 874 (1957).
- ²H. R  ther, *Surface Plasmons on Smooth and Rough Surfaces and on Gratings* (Springer-Verlag, Berlin, 1988).
- ³R.W. Wood, Proc. R. Soc. London, Ser. A **18**, 269 (1902).
- ⁴U. Fano, J. Opt. Soc. Am. **31**, 213 (1941).
- ⁵A. Hessel and A.A. Oliner, Appl. Opt. **4**, 1275 (1965).
- ⁶A. Wirgin and T. L  pez-R  os, Opt. Commun. **48**, 416 (1984); **49**, 455(E) (1984); T. L  pez-R  os and A. Wirgin, Solid State Commun. **52**, 197 (1984).
- ⁷T. L  pez-R  os, D. Mendoza, F.J. Garc  a-Vidal, J. S  nchez-Dehesa, and B. Pannetier, Phys. Rev. Lett. **81**, 665 (1998); F.J. Garc  a-Vidal, J. S  nchez-Dehesa, A. Dechelette, E. Bustarret, T. L  pez-R  os, Th. Fournier, and B. Pannetier, J. Lightwave Technol. **17**, 2191 (1999).
- ⁸W.L. Barnes, T.W. Preist, S.C. Kitson, and J.R. Sambles, Phys. Rev. B **54**, 6227 (1996); S.C. Kitson, W.L. Barnes, and J.R. Sambles, Phys. Rev. Lett. **77**, 2670 (1996).
- ⁹R.A. Watts, T.W. Preist, and J.R. Sambles, Phys. Rev. Lett. **79**, 3978 (1997); M.B. Sobnack, W.C. Tan, N.P. Wanstall, T.W. Preist, and J.R. Sambles, *ibid.* **80**, 5667 (1998); N.P. Wanstall, W.C. Tan, T.W. Preist, M.B. Sobnack, and J.R. Sambles, J. Opt. Soc. Am. A **15**, 2869 (1998).
- ¹⁰H. Lochbihler and R.A. Depine, Appl. Opt. **32**, 3459 (1993); H. Lochbihler, Phys. Rev. B **50**, 4795 (1994).
- ¹¹J.J. Kuta, H. M. van Driel, D. Landheer, and Y. Feng, J. Opt. Soc. Am. A **12**, 1118 (1995).
- ¹²T.W. Ebbesen, H. J. Lezec, H. F. Ghaemi, T. Thio, and P. A. Wolff, Nature (London) **391**, 667 (1998).
- ¹³U. Schr  ter and D. Heitmann, Phys. Rev. B **58**, 15 419 (1998).
- ¹⁴M.M.J. Treacy, Appl. Phys. Lett. **75**, 606 (1999).
- ¹⁵J.A. Porto, F.J. Garc  a-Vidal, and J.B. Pendry, Phys. Rev. Lett. **83**, 2845 (1999).
- ¹⁶Y. Takakura, Phys. Rev. Lett. **86**, 5601 (2001).
- ¹⁷Ph. Lalanne, J.P. Hugoin, S. Astilean, M. Palamaru, and K.D. Moller, J. Opt. A: Pure Appl. Opt. **2**, 48 (2000); E. Popov, M. Nevriere, S. Enoch, and R. Reinisch, Phys. Rev. B **62**, 16 100 (2000); S. Collin, F. Pardo, R. Teissier, and J.-L. Pelouard, *ibid.* **63**, 033107 (2001).
- ¹⁸H.E. Went, A.P. Hibbins, J.R. Sambles, C.R. Lawrence, and A.P. Crick, Appl. Phys. Lett. **77**, 2789 (2001).
- ¹⁹J.B. Pendry, J. Mod. Opt. **41**, 209 (1994); P.M. Bell, J. B. Pendry, L. Mart  n-Moreno, and A. J. Ward, Comput. Phys. Commun. **85**, 306 (1995).
- ²⁰F.J. Garc  a-Vidal and J.B. Pendry, Phys. Rev. Lett. **77**, 1163 (1996).
- ²¹P. Sheng, R.S. Stepleman, and P.N. Sanda, Phys. Rev. B **26**, 2907 (1982).
- ²²L. Mart  n-Moreno, F.J. Garc  a-Vidal, H.J. Lezec, K.M. Pellerin, T. Thio, J.B. Pendry, and T.W. Ebbesen, Phys. Rev. Lett. **86**, 1114 (2001); A. Krishnan, T. Thio, T.J. Kim, H.J. Lezec, T.W. Ebbesen, P.A. Wolff, J.B. Pendry, L. Mart  n-Moreno, and F.J. Garc  a-Vidal, Opt. Commun. **200**, 1 (2001).